catalysts

MDPI

Article

N Doped Activated Biochar from Pyrolyzing Wood Powder for Prompt BPA Removal via Peroxymonosulfate Activation

Haiqin Lu [1], Guilu Xu [1] and Lu Gan [1,2,*]

[1] College of Materials Science and Engineering, Nanjing Forestry University, Nanjing 210037, China
[2] Jiangsu Co-Innovation Center of Efficient Processing and Utilization of Forest Resources, International Innovation Center for Forest Chemicals and Materials, College of Materials Science and Engineering, Nanjing Forestry University, Nanjing 210037, China
* Correspondence: ganlu@njfu.edu.cn

Abstract: In the present study, nitrogen doped biochar (N-PPB) and nitrogen doped activated biochar (AN-PPB) were prepared and used for removing bisphenol A (BPA) in water through activating peroxymonosulfate. It was found from the results that N-PPB exhibited superior catalytic performance over pristine biochar since nitrogen could brought about abundant active sites to the biochar structure. The non-radical singlet oxygen ($^1O_2$) was determined to be the dominant active species responsible for BPA degradation. Having non-radical pathway in the N-PPB/PMS system, the BPA degradation was barely influenced by many external environmental factors including solution pH value, temperature, foreign organic, and inorganic matters. Furthermore, AN-PPB had richer porosity than N-PPB, which showed even faster BPA removal efficiency than N-PPB through an adsorptive/catalytic synergy. The finding of this study introduces a novel way of designing hieratical structured biochar catalysts for effective organic pollutant removal in water.

Keywords: nitrogen dope; biochar; peroxymonosulfate; KOH activation; bisphenol A degradation

Citation: Lu, H.; Xu, G.; Gan, L. N Doped Activated Biochar from Pyrolyzing Wood Powder for Prompt BPA Removal via Peroxymonosulfate Activation. *Catalysts* **2022**, *12*, 1449. https://doi.org/10.3390/catal12111449

Academic Editors: Hao Xu and Yanbiao Liu

Received: 28 October 2022
Accepted: 14 November 2022
Published: 16 November 2022

1. Introduction

In recent years, advanced oxidation processes (AOPs) based on persulfate activations have been widely studied for catalytic degradation of organic contaminants [1,2]. Amongst various approaches for activating persulfate, transitional metal ions or metal compounds exhibit superior efficiency [3]. Nevertheless, it is intractable to overcome the metal ion leaching issue which can cause serious environmental pollution problems [4]. Recent studies have shown that carbonaceous materials can also effectively activate persulfate [5]. Thereinto, wood-derived biochar produced from pyrolyzing biomass precursor in low-oxygen or oxygen-free atmosphere has received tremendous research interest due to the advantages of abundant existence, low cost, low biotoxicity, and good stability, as well as numerous active oxygen-containing functional groups [6,7].

However, pristine biochar has low the degradation efficiency and poor recycling performance due to its limited active sites within skeletons for persulfate activation [8]. Nitrogen doping is considered to be an effective method to improve the catalytic capability of biochar through introducing diverse N-containing functional groups (pyridine N, pyrrole N, graphitic N) on the surface of biochar [9], which can not only change the electron density of local carbon atoms and increase electron mobility, but also increase edge defects of biochar [10]. At the same time, N atoms can also adjust the surface chemical properties through changing the charge/spin distribution of biochar, improve the adsorption capacity of persulfate, and add extra active sites [11], which are all in favor of catalytic degradations of organic pollutants [12]. On the other hand, biochar can be converted to activated carbon by an activation agent, through which biochar can have more surface oxygen functional groups, higher defects degree of internal carbon structure, and richer porosity [13]. Furthermore, the resulted activated biochar can be endowed with immensely

increase the specific surface area along with hierarchical pore structures, which promote the adsorption capability of the biochar [14]. Therefore, it is potential to obtain N-doped activated biochar which have high organic pollutant removal efficiency in water through adsorption/degradation synergy through combining N doping and activating modification treatments to wood-based biochar.

Thus, in this study, N-doped biochar catalysts with different pyrolysis temperatures (450 °C, 600 °C, 750 °C, 900 °C) were prepared using industrial poplar powder as precursor and urea as nitrogen source. After comparing the catalytic performance through degrading bisphenol A (BPA) via activating peroxymonosulfate (PMS), the biochar pyrolyzed at 750 °C with optimal performance was then selected to prepare N-doped activated biochar using KOH as activating agent. The performance of N-doped activated biochar/PMS system towards BPA degradation was studied systematically afterwards. Furthermore, the recyclability and actual water adaptability of the reaction system were also investigated. The BPA degradation mechanisms in the reaction system were also analyzed.

2. Results and Discussion

The surface morphology structure difference between pristine poplar powder and N-PPB investigated in terms of SEM with the results shown in Figure 1. It could be observed from Figure 1a that pristine poplar powder displayed a smooth strip shape. After pyrolysis treatment, and nitrogen doping, N-PPB750 exhibited a rougher structure with richer porosity (Figure 1b), which was considerably distinguished from pristine poplar powder. At the same time, the particles of N-PPB750 became smaller compared with that of pristine poplar powder, which was attributed to the decomposition of lignocellulose component in the poplar powder during pyrolysis process [15]. The pyrolysis treatment also promoted the exfoliation of the carbon layers, which lead to the formation of abundant pores. The EDS elemental mapping diagrams shown in Figure 1d–f demonstrated that several main elements including C, N, and O were uniformly distributed N-PPB750. The contents of three major elements shown in Table 1 illustrated that a quite high content of N element (17.98 wt%) imported by urea precursor was anchored in the biochar structures.

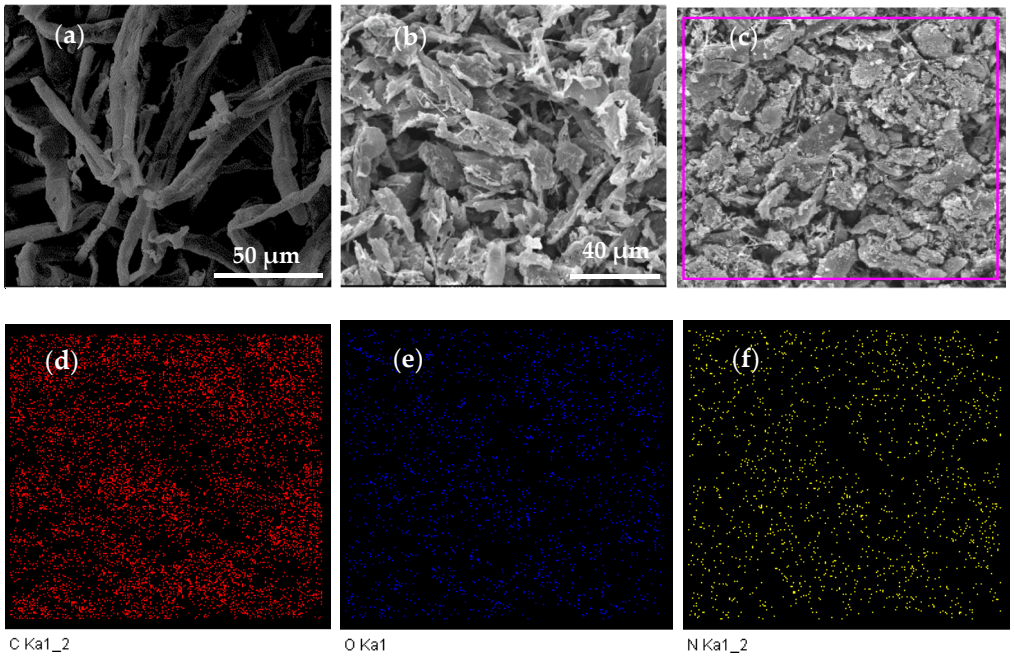

Figure 1. SEM images of (**a**) PPB-750, (**b**) N-PPB750, (**c**) selected area of N-PPB750 (red box) for EDS elemental mapping and EDS elemental mapping of (**d**) C, (**e**) O, (**f**) N.

Table 1. Elemental ratio of N-PPB750 (C, O, N).

Element	Weight%	Atomic%
C K	50.52	56.40
N K	17.98	17.21
O K	31.50	26.39
Totals	100.00	

The structures of N-PPB samples were then identified through XRD analysis with the results shown in Figure 2a. It could be seen that the pristine poplar powder had three wide diffraction peaks at 2θ = 15°, 22°, and 35°, which were affiliated to the Cellulose I structure of typical wood based biomass materials [16]. After pyrolysis, these three peaks were replaced by two broad peaks located at ~26° and 42° in N-PPB samples, which corresponded to (002) and (110) planes of classic carbon materials with graphitic structures [17]. These results further indicated the formation of fine graphitic structure in the prepared N-PPB samples. Additionally, many sharp small peaks in the range of 22–40° were also observed in all tested samples, which were related to the mineral salts such as calcium carbonate and silica existed in natural poplar powder [18]. These peaks became weaker with the elevation of pyrolysis temperature, which might be because some of the mineral salts were evaporated at higher temperature.

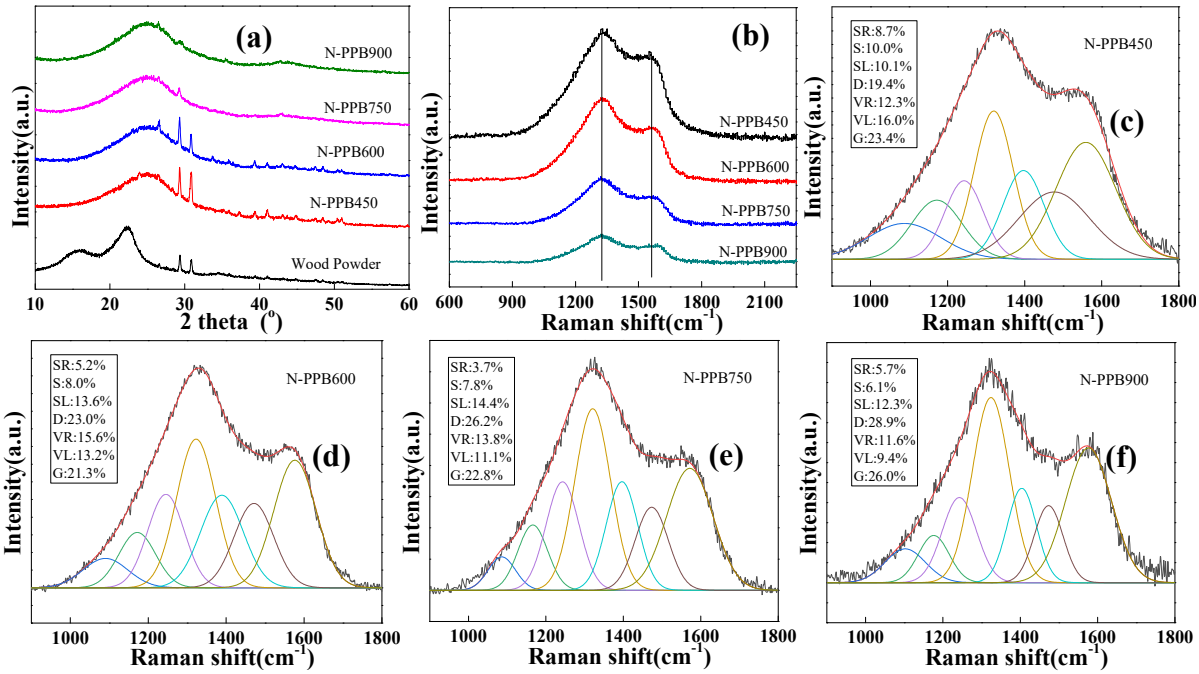

Figure 2. (**a**) XRD patterns, (**b**) Raman spectra, and (**c**–**f**) deconvoluted Raman spectra of N-PPB450, N-PPB600, N-PPB750, N-PPB900.

Figure 2b–f shows the Raman spectra of the N-PPB samples. As shown in Figure 2b, two characteristic peaks located at 1360 cm^{-1} and 1580 cm^{-1} could be observed for all the N doped biochar samples, which were ascribed to the characteristic D band and G band of a graphitic carbonaceous material [19]. This meant poplar wood could be converted to carbonaceous biochar when the pyrolysis temperature was higher than 450 °C. After the Raman spectra was deconvoluted, it was seen that the spectrum of each N-PPB sample were consisted of seven characteristic peaks which were ascribed to were divided into the SR band representing C-H on aromatic rings (1086 cm^{-1}), the S band representing $C_{aromatic}$-C_{alkyl} (1170 cm^{-1}), the SL band representing C_{aryl}-O-C_{alkyl} (1245 cm^{-1}), the D band representing the defective and disordered arrangement of carbon atoms (1320 cm^{-1}), the VR

band representing to amorphous carbon and deterioration of crystallinity (1390 cm^{-1}), the VL band representing the semicircle ring breathing (1468 cm^{-1}), and the G band representing in-plane stretching vibration of C atomic sp^2 hybridization (1576 cm^{-1}), respectively [20]. The area ratio between D band and G band (A_D/A_G) was generally used to characterize the defect degree of the graphitic structure in a carbonaceous material [21]. It was seen that the A_D/A_G value increased from 0.83 to 1.15 with the increase in the pyrolysis temperature, indicating that higher pyrolysis temperature brought about more defect to the biochar. In the meantime, the area ratio between D band and (VR+VL) bands (A_D/A_V) represented the defect density of boundary edges in the carbon. It was seen that all the biochar samples had an A_D/A_V value of lower than 3.5, indicating that the prepared N-PPB samples were considered to contain a higher density defect of boundary edges with more unsaturated carbon atoms and a lower degree of graphitization [22].

XPS analysis was then conducted to further explore the surface element composition of the prepared N-PPB. As illustrated in Figure 3a, the main elements of C, N, and O were all observed in the spectra of the biochar samples, in which the concentration of N decreased significantly with the increase in the pyrolysis temperature. Figure 3b–d reveals the deconvoluted C1s, O1s, and N1s spectra. It was observed from Figure 3b that C1s spectrum was mainly composed of four peaks located at 284.5 eV, 285.2 eV, 286.2 eV, and 288.8 eV, which represented the C=C/C-C, C–O, C=O and COOH bonding, respectively [23,24]. Similarly, the O1s spectrum could be divided into C=O (530.9 eV), C-O (532.2 eV), and COOH (533.6 eV) (Figure 3c), and N1s spectra could be deconvoluted into four peaks corresponding to pyridinic—N (398.3 eV), pyrrolic—N (399.5 eV), graphite—N (400.4 eV), and −NOx (401.4 eV) (Figure 3d) [25]. The detailed concentrations of respective bonding were listed in Table 2. As shown, the concentration of C=C/C-C decreased with the increment of pyrolysis temperature from 450 °C to 900 °C, which was in agreement with the Raman results. Correspondingly, the proportion of C=O bonding increased with the increase in the pyrolysis temperature, which could be resulted from the conversion of C=C/C-C bonding. As for N1s bonding, the conversion of pyrrolic N or pyridine N to graphitic N could be obviously seen.

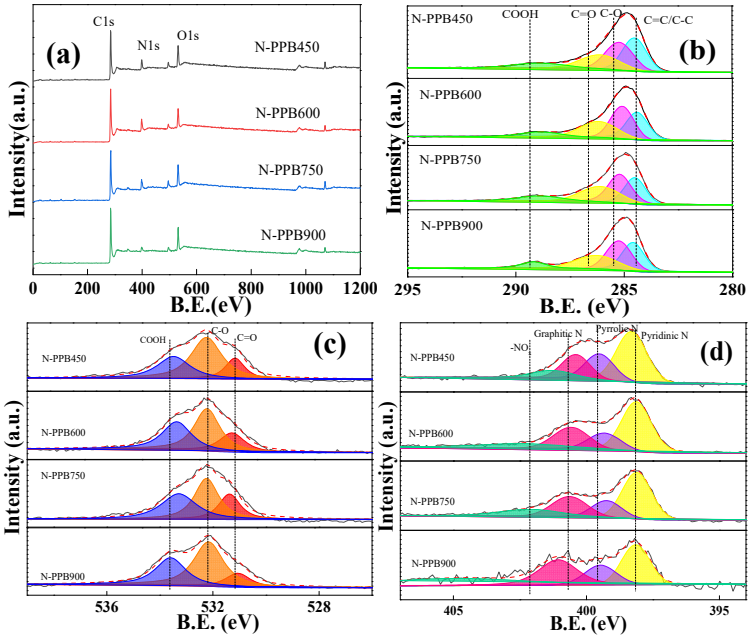

Figure 3. (**a**) Wide-scan XPS spectra, high resolution (**b**) C 1s, (**c**) N 1s, (**d**) O 1s spectra of N-PPB catalysts.

Table 2. Bonding ratio of N-PPB samples based on deconvoluted C1s and N1s XPS peak.

	C1s				N1s, %			
	C=C/C-C	C-O	C=O	–COOH	Pyridinic N	Pyroolic N	Graphitic N	$-NO_x$
N-PPB450	33.2%	32.0%	23.7%	11.1%	47.9%	22.8%	20.2%	9.1%
N-PPB600	30.7%	34.2%	26.8%	8.3%	46.6%	17.2%	21.4%	14.8%
N-PPB750	27.2%	34.5%	28.1%	10.2%	45.1%	16.8%	22.6%	15.5%
N-PPB900	31.7%	33.4%	26.4%	8.5%	31.0%	17.6%	27.5%	23.9%

The catalytic performance of the prepared N-PPB samples was investigated through degrading BPA in water with the results shown Figure 4a. As illustrated, the PPB samples showed negligible adsorption activity towards BPA since the biochar was not activated. Moreover, nitrogen doping could significantly enhance the PMS activation capability of the biochar, and all the N-PPB samples (0.5 g/L) could completely degrade 0.02 mM BPA in the solution. Within the same time span, PPB without N doping could only degrade ~10% of BPA. This indicated that N doping significantly enriched the active sites on PPB surface, which accelerated the PMS activation efficiency of the biochar sample. It was also seen that the activation capability of the N-PPB sample increased with the pyrolysis temperature, and when pyrolysis temperature increased to 600 °C or higher, the catalytic performance of the corresponding PPB did not increase much. The TOC results obtained from N-PPB600/PMS system indicated that when the reaction time was extended to 30 min, ~58% of the TOC could be removed. This result implied that the BPA could be degraded into small molecules by the prepared N-PPB catalysts and finally mineralized into inorganic molecules.

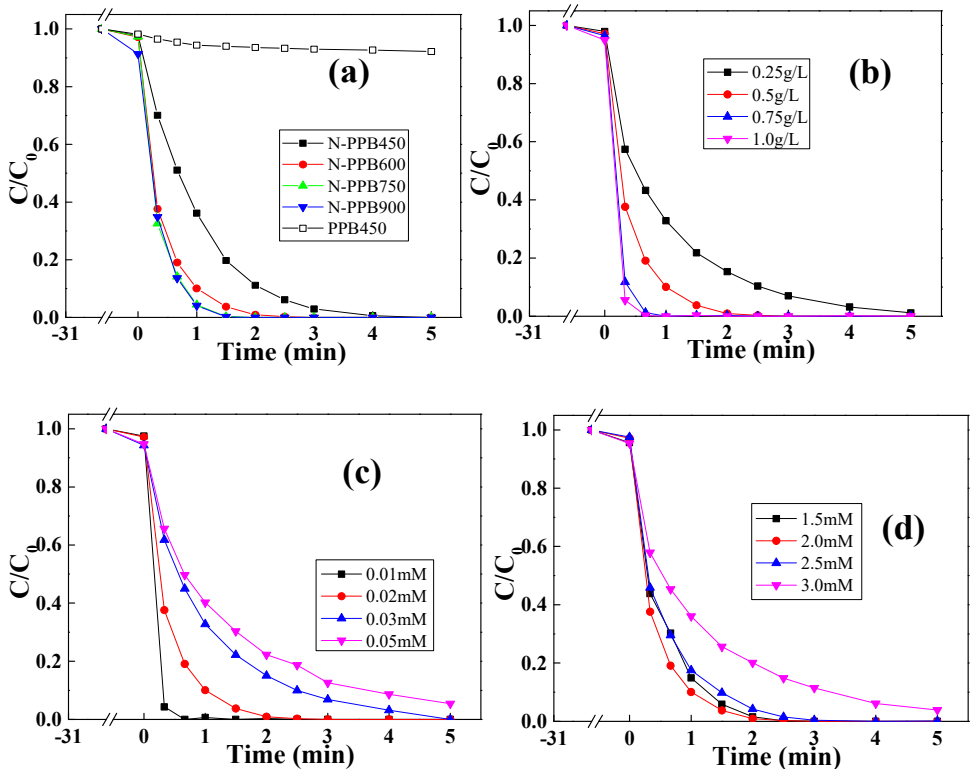

Figure 4. (**a**) Catalytic performance of N-PPB samples ($[catalyst]_0$ = 0.5 g/L, $[BPA]_0$ = 0.02 mM, $[PMS]_0$ = 1.5 mM), impact of (**b**) catalyst dosage ([BPA]0 = 0.02 mM, $[PMS]_0$ = 1.5 mM), (**c**) BPA concentration ($[catalyst]_0$ = 0.5 g/L, $[PMS]_0$ = 1.5 mM), and (**d**) PMS concentration on the performance of N-PPB600 ($[catalyst]_0$ = 0.5 g/L, $[BPA]_0$ = 0.02 mM).

N-PPB600 was selected for the following test. The impact of reaction parameters, including BPA concentration, catalyst dosage, and PMS concentration on the performance of

N-PPB600, was then investigated with the results shown in Figure 4b–d. It was revealed that the catalytic performance of N-PPB600 had a positive correlation with the catalyst dosage, and had a negative correlation with the BPA concentration. It was easy to understand that increased catalyst dosage could increase the number of active sites for PMS activation, which led to the increase in active species for BPA degradation [26]. Conversely, when the concentrations of both N-PPB600 and PMS were fixed, a constant number of active species was insufficient to degrade increased amount of BPA molecules, which resulted in the performance decline of N-PPB600. While when the concentration of PMS was increased in the reaction solution, the performance of N-PPB600 increased when PMS concentration increased from 1.5 mM to 2.0 mM, and declined when further increasing the PMS concentration. This might because an excessive amount of PMS would also consume the generated active species, which inhibited the BPA degradation [27].

The impact of solution parameters on the performance of N-PPB600 was investigated afterwards. Figure 5a shows the influence of solution pH on the BPA degradation efficiency. Overall, the catalytic performance of N-PPB600 was not much influenced by the fluctuation of solution pH value, indicating promising performance stability of the catalyst. It was further observed from Figure 5b that the activity of N-PPB600 boosted with the increase in the system temperature, indicating the endothermic nature of the PMS activation process [28].

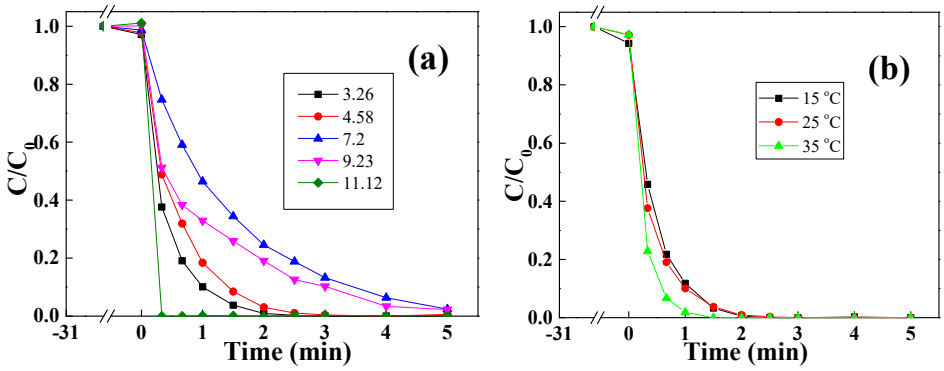

Figure 5. Impact of (**a**) pH value and (**b**) solution temperature on the performance of N-PPB600 ($[catalyst]_0$ = 0.5 g/L, $[BPA]_0$ = 0.02 mM, $[PMS]_0$ = 1.5 mM).

Figure 6 shows the impact of foreign matters including inorganic anions, natural organic matters and complex water matrices on the performance of the biochar catalyst. As illustrated in Figure 6a–d, all inorganic anions could influence the activity of N-PPB600. Specifically, $H_2PO_4^-$, HCO_3^-, and NO_3^- inhibited the BPA degradation efficiency since these anions would occupy the catalyst surface and hinder the contact between the active sites in the catalyst and PMS, resulting lower active species generation rate [29]. Unlike the other three anions, the dosage of Cl^- sped up the BPA degradation rate, and the increased amount of Cl^- would accelerate the BPA degradation rate more intensely. This was because Cl^- could react with PMS and active species and generate more chlorine based species [30], which, as a result, boosted the removal efficiency of BPA in the reaction system. It was also seen from Figure 6e–f that both humic acid and natural water had an impediment effect on the catalytic activity of N-PPB600, which was ascribed to the similar reason to the anions as discussed above. It has to be noted that even the concentration of the anions and humic acid increased to as high as 50 mM; 0.02 mM of BPA could still be effectively degraded with high removal rate, implying promising water matrix adaptability of the prepared catalyst.

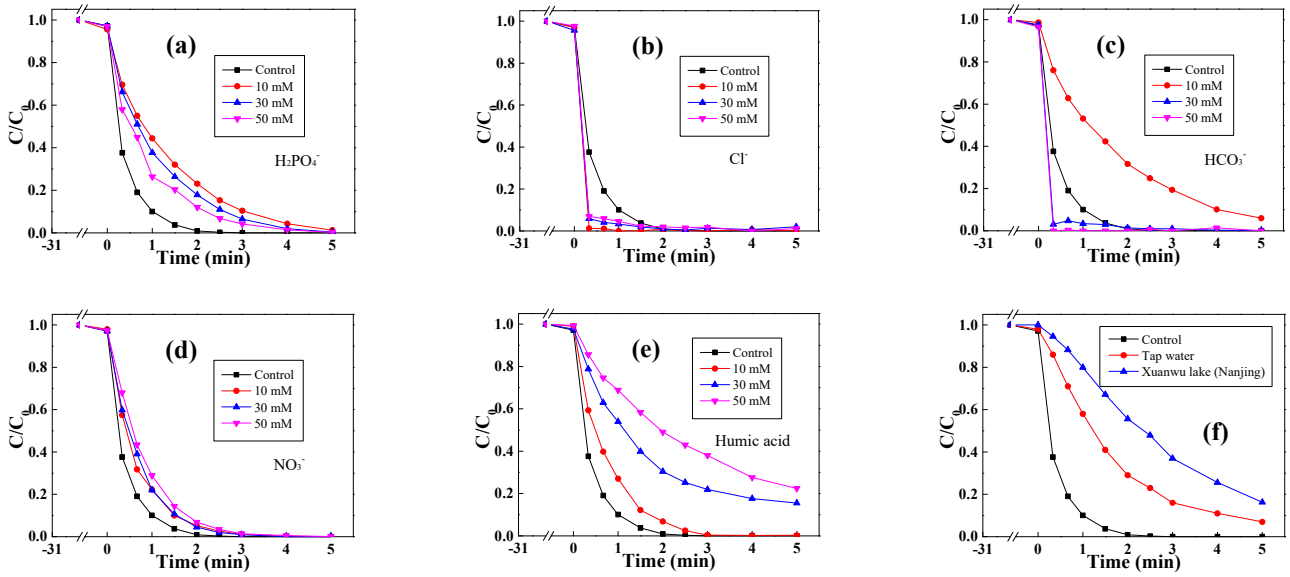

Figure 6. Impact of (**a**) $H_2PO_4^-$, (**b**) Cl^-, (**c**) HCO_3^-, (**d**) NO_3^-, (**e**) humic acid, and (**f**) natural water on the performance of N-PPB600 ([catalyst]$_0$ = 0.5 g/L, [BPA]$_0$ = 0.02 mM, [PMS]$_0$ = 1.5 mM).

The active species generated in the reaction system which dominated the BPA degradation was investigated through scavenging test with the results shown in Figure 7a. It was observed that both methanol (MeOH) and tert-butyl alcohol (TBA) did not show any inhibition effect to BPA degradation, indicating that no radical species was generated in the reaction system. When the trapping agent was changed to L-histidine and parabenzoquinone (p-BQ), the BPA degradation could be completely inhibited. Since these two agents were both non-radical scavenger which could effectively trap singlet oxygen ($^1O_2$) in the solution [31], this meant the N-PPB600/PMS system was a $^1O_2$ dominated system for BPA degradation. This could also explain why N-PPB600 could kept its catalytic activity at various water matrices since $^1O_2$ was not much influenced by the variation of external environment.

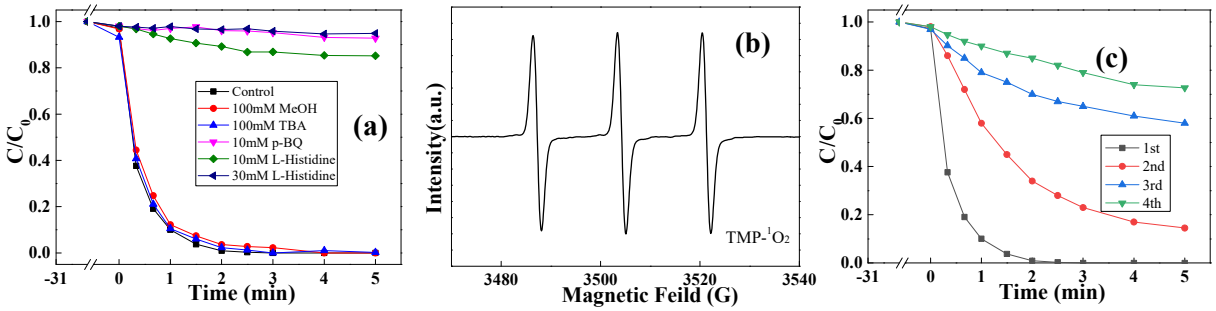

Figure 7. (**a**) BPA degradation in N-PPB600/PMS system at the existence of various scavengers, (**b**) ESR spectra test, (**c**) recyclability test for N-PPB600 ([catalyst]$_0$ = 0.5 g/L, [BPA]$_0$ = 0.02 mM, [PMS]$_0$ = 1.5 mM).

The ESR results shown in Figure 7b also illustrated that when using TMP as the trapping agent, a clear triplet peak which was ascribed to the typical TMP-$^1O_2$ adduct could be observed, indicating that abundant $^1O_2$ was existed in the N-PPB600/PMS system. Many previous studies indicated that the electron-rich Lewis basic sites in biochar could transfer the electrons to PMS and caused the generation of non-radical $^1O_2$ [32]. Since nitrogen doping could introduce abundant electron-rich nitrogen containing groups to the biochar including pyridinic N and pyrrolic N [33], the N-PPB600 could exhibited higher PMS activating efficiency than the pristine biochar.

The catalytic stability of N-PPB600 was investigated afterwards. It was seen from Figure 7c that the catalytic capability of the biochar gradually reduced after four consecutive runs, which indicated that the active sites on the catalyst surface was continuously consumed when activating PMS. Thus, the XPS spectra of the recycled N-PPB600 was investigated to illustrate the PMS activation mechanism with the results shown in Figure 8. As shown in Figure 8a, the N element was significantly consumed after consecutive BPA degradation cycles, indicating that N doping played a critical role of improving the catalytic properties of the biochar. From the deconvoluted C1s, N1s, and O1s spectra shown in Figure 8b–d, it was seen that the concentrations of C=O, pyridinic N and graphitic N were reduced after the reaction cycles, implying that these bonding participated the PMS activation and were consumed gradually, which were in accordance with many previous studies [34].

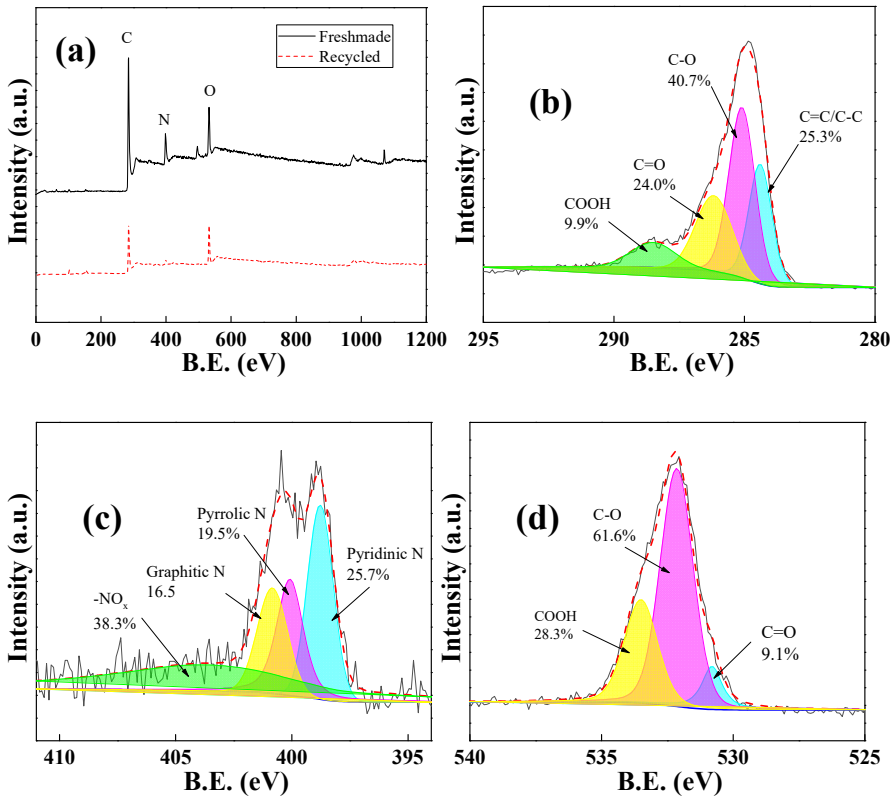

Figure 8. (**a**) Wide-scan XPS spectra, (**b**) C 1s, (**c**) N 1s, (**d**) O 1s spectra of used N-PPB600.

To improve the BPA degradation efficiency of the biochar, AN-PPB600 was prepared to enhance the adsorption capability of the biochar. It was seen that AN-PPB600 had much higher specific surface area and pore volume than N-PPB600 after KOH activation (Table 3), which indicated that AN-PPB600 should have better adsorption capability than N-PPB600. As illustrated in Figure 9, ~80% of BPA could be adsorbed by AN-PPB600 at the first 30 min, while no more than 10% of BPA was adsorbed by N-PP600. When PMS was dosed, 0.5 g/L of AN-PPB600 could completely remove BPA with high concentration of 0.1 mM through adsorptive/catalytic synergy within 3 min. Conversely, N-PPB600 could only degrade ~15% of BPA within the same time span. This indicated that through designing hieratical structured biochar with both high adsorptive and catalytic capability, organic pollutants in water could be promptly removed through the synergetic process.

Table 3. Specific surface area and pore volume of N-PPB600 and AN-PPB600.

Sample	Specific Surface Area ($m^2 \cdot g^{-1}$)	Pore Volume ($cm^3\ g^{-1}$)
N-PPB600	141	0.203
AN-PPB600	855	1.683

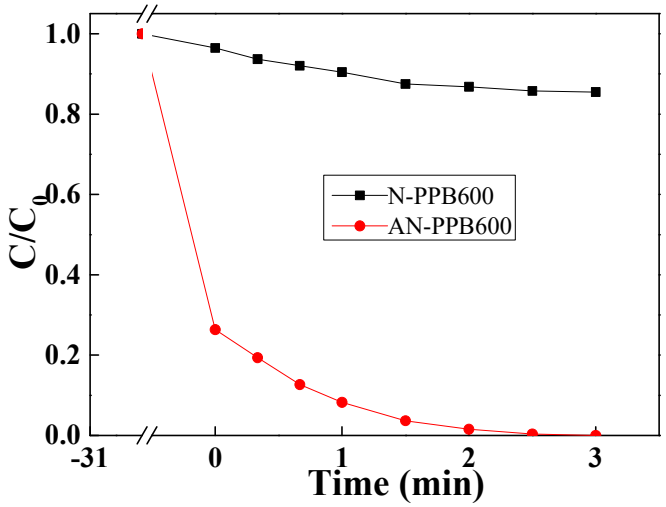

Figure 9. BPA degradation in N-PPB600/PMS and AN-PPB600/PMS systems ($[catalyst]_0$ = 0.5 g/L, $[BPA]_0$ = 0.02 mM, $[PMS]_0$ = 1.5 mM).

3. Experimental

3.1. Reagents and Chemicals

Poplar powder (300 mesh) was obtained from Yixing wood powder factory (Linyi, China). PMS (Oxone, $KHSO_5 \cdot 0.5KHSO_4 \cdot 0.5K_2SO_4$) and BPA (99%) were purchased from Sigma-Aldrich (St. Louis, MO, USA). Urea (CH_4N_2O, 99%) was provided from Nanjing Chemical Reagent Co., Ltd. (Nanjing, China). 2,2,6,6-tetramethyl-4-piperidine (TMP, 98%) was acquired from Aladdin (Shanghai, China). All the other chemicals and reagents were of analytical grade and used without further purification. Double distilled water (H_2O) was utilized throughout the whole experiments.

3.2. Preparation of the Catalysts

Typically, 3.0 g urea was first dissolved into 20 mL H_2O, after which 1.0 g poplar powder was added. The mixture was magnetically stirred 70 °C until all the H_2O was evaporated. Afterwards, the obtained powder was put into a tubular furnace, heated to desired temperature (450 °C, 600 °C, 750 °C and 900 °C) under N_2 atmosphere at 5 °C/min, pyrolyzed at respective temperature for 3 h. After cooling to room temperature, the obtained solid was further washed with H_2O for several times until the pH value of H_2O reached ~7. After being dried in an oven at 60 °C for 24 h, N-doped biochar derived from poplar powder was obtained, and was designated to be N-PPBx, where x represented the pyrolysis temperature. For comparison, activated N-doped biochar was synthesized via a similar route except that 2.0 g KOH was also dissolved in urea solution in the first step, which was named as AN-PPBx.

3.3. Characterizations

The morphology of biochar was investigated by scanning electron microscope (SEM, JEOL SEM 6490, Tokyo, Japan). The crystalline structures were studied by X-ray diffraction diffractometer (XRD, Rigaku Smartlab, Tokyo, Japan). Raman spectra of the prepared samples was investigated by a Raman spectrometer equipped with an Ar laser (532 nm, 180 mW) (Horiba Jobin Yvon HR800Tokyo, Japan). X-ray photoelectron spectroscopy (XPS,

Kratos Ultra DLD, Warwick, UK) was used to detect surface chemistry and element composition. Electron spin resonance spectroscopy (ESR, Bruker EMX-10/12, Bremen, Germany) was used to identify generated reactive oxygen species (ROS) in the biochar/PMS system. Electrochemical measurements were carried out with a CHI760E electrochemical workstation. The concentration of BPA was analyzed by high performance liquid chromatography (HPLC, Dionex Ultimate 3000, Sunnyvale, CA USA) equipped with C18 column (5 μm particle size, 250 × 4.6 mm) and UV detector at 278 nm. Total organic carbon (TOC) was measured by a MutiN/C 2100 analyzer (Jena, Germany).

3.4. Degradation Process

All the catalytic degradation experiments were conducted in a glass beaker containing 100 mL BPA solution with continuous mechanical stirring. In brief, a certain amount of biochar sample was first dispersed in H_2O and sonicated for 30 min to obtain a uniform dispersion. Afterwards, BPA solution with pre-determined concentration was obtained through injecting a certain amount of BPA stock solution into the dispersion. Before PMS was dosed to initiate BPA degradation, the mixture was stirred for 30 min to achieve the adsorption/desorption equilibrium. During the BPA degradation process, 1 mL of solution sample was periodically extracted from the reaction system, filtered with a 0.22 μm polytetrafluoroethylene membrane, and quenched with 0.5 mL methanol. The initial pH value of the solution was measured after PMS and catalyst were added, and was adjusted by NaOH (1 M) and H_2SO_4 (1 M). In a recycling test, the used biochar was separated from the reaction system through centrifuging, which was then rinsed 3 times with clean H_2O and dried at 60 °C for 12 h before being dosed to initiate next BPA degradation cycle. The ROS produced during oxidative degradation of pollutants were identified by scavenging experiments using methanol (MeOH), isobutanol (TBA), p-benzoquinone (p-BQ), and L-histdine (His) as scavengers. All experiments were conducted in triplicates, and the data were the mean values with standard deviations.

4. Conclusions

To conclude, N-PPB catalysts were prepared and used for the removal of BPA in water through activating PMS. The results shows that nitrogen doping could significantly enhance the catalytic performance of pristine biochar, in which 0.02 mM of BPA could be completely degraded within 5 min by 0.5 g/L of biochar catalyst. The scavenging test showed that non-radical $^1O_2$ was the main active species which dominated the BPA degradation. Due to this reason, the N-PPB/PMS system showed promising water matrix adaptability. To enhance the BPA removal efficiency, KOH was introduced to activate N-PPB, and the results illustrated that AN-PPB could promptly remove high concentration BPA in water through adsorptive/catalytic synergy. This study provides a new thinking of preparing biochar catalyst with heteroatom doing and hieratical structure design, which could remove organic pollutants in water with high efficiency.

Author Contributions: Investigation, writing—original draft preparation, data curation, H.L.; visualization, formal analysis, G.X.; writing—review and editing, supervision, funding acquisition, L.G. All authors have read and agreed to the published version of the manuscript.

Funding: This research was funded by the Natural Science Foundation of Jiangsu Province, China (BK20201385).

Data Availability Statement: Data are available upon request.

Acknowledgments: The Advanced Analysis and Testing Center of Nanjing Forestry University is acknowledged.

Conflicts of Interest: The authors declare no conflict of interest.

References

1. Shi, J.; Dai, B.; Fang, X.; Xu, L.; Wu, Y.; Lu, H.; Cui, J.; Han, S.; Gan, L. Waste preserved wood derived biochar catalyst for promoted peroxymonosulfate activation towards bisphenol A degradation with low metal ion release: The insight into the mechanisms. *Sci. Total Environ.* **2022**, *813*, 152673. [CrossRef] [PubMed]
2. Lv, Y.; Zong, L.; Liu, Z.; Du, J.; Wang, F.; Zhang, Y.; Ling, C.; Liu, F. Sequential separation of Cu(II)/Ni(II)/Fe(II) from strong-acidic pickling wastewater with a two-stage process based on a bi-pyridine chelating resin. *Chin. Chem. Lett.* **2021**, *32*, 2792–2796. [CrossRef]
3. Sethi, Y.A.; Panmand, R.P.; Ambalkar, A.; Kulkarni, A.K.; Patil, D.R.; Gunjal, A.R.; Gosavi, S.W.; Kulkarni, M.V.; Kale, B.B. *In situ* preparation of CdS decorated $ZnWO_4$ nanorods as a photocatalyst for direct conversion of sunlight into fuel and RhB degradation. *Sustain. Energy Fuels* **2019**, *3*, 793–800. [CrossRef]
4. Pan, Y.; Bu, Z.; Sang, C.; Guo, H.; Zhou, M.; Zhang, Y.; Tian, Y.; Cai, J.; Wang, W. EDTA enhanced pre-magnetized Fe_0/H_2O_2 process for removing sulfamethazine at neutral pH. *Sep. Purif. Technol.* **2020**, *250*, 117281. [CrossRef]
5. Lu, H.; Gan, L. Catalytic Degradation of Bisphenol A in Water by Poplar Wood Powder Waste Derived Biochar via Peroxymonosulfate Activation. *Catalysts* **2022**, *12*, 1164. [CrossRef]
6. Zhao, Z.; Zhang, X.; Lin, Q.; Zhu, N.; Gui, C.; Yong, Q. Development and investigation of a two-component adhesive composed of soybean flour and sugar solution for plywood manufacturing. *Wood Mater. Sci. Eng.* **2022**, 1–9. [CrossRef]
7. Zuo, S.; Zhang, W.; Wang, Y.; Xia, H. Low-Cost Preparation of High-Surface-Area Nitrogen-Containing Activated Carbons from Biomass-Based Chars by Ammonia Activation. *Ind. Eng. Chem. Res.* **2020**, *59*, 7527–7537. [CrossRef]
8. Bhatia, S.K.; Gurav, R.; Choi, T.-R.; Kim, H.J.; Yang, S.-Y.; Song, H.-S.; Park, J.Y.; Park, Y.-L.; Han, Y.-H.; Choi, Y.-K.; et al. Conversion of waste cooking oil into biodiesel using heterogenous catalyst derived from cork biochar. *Bioresour. Technol.* **2020**, *302*, 122872. [CrossRef]
9. You, Y.; Zhao, Z.; Song, Y.; Li, J.; Li, J.; Cheng, X. Synthesis of magnetized nitrogen-doped biochar and its high efficiency for elimination of ciprofloxacin hydrochloride by activation of peroxymonosulfate. *Sep. Purif. Technol.* **2020**, *258*, 117977. [CrossRef]
10. Başẗurk, E.; Alver, A. Modeling azo dye removal by sono-fenton processes using response surface methodology and artificial neural network approaches. *J. Environ. Manag.* **2019**, *248*, 109300. [CrossRef]
11. Ye, S.; Zeng, G.; Tan, X.; Wu, H.; Liang, J.; Song, B.; Tang, N.; Zhang, P.; Yang, Y.; Chen, Q.; et al. Nitrogen-doped biochar fiber with graphitization from Boehmeria nivea for promoted peroxymonosulfate activation and non-radical degradation pathways with enhancing electron transfer. *Appl. Catal. B Environ.* **2020**, *269*, 118850. [CrossRef]
12. Huang, B.-C.; Jiang, J.; Huang, G.-X.; Yu, H.-Q. Sludge biochar-based catalysts for improved pollutant degradation by activating peroxymonosulfate. *J. Mater. Chem. A* **2018**, *6*, 8978–8985. [CrossRef]
13. Liu, X.; Zuo, S.; Cui, N.; Wang, S. Investigation of ammonia/steam activation for the scalable production of high-surface area nitrogen-containing activated carbons. *Carbon* **2022**, *191*, 581–592. [CrossRef]
14. Gao, H.; Zuo, S.; Wang, S.; Xu, F.; Yang, M.; Hu, X. Graphitic crystallite nanomaterials enable the simple and ultrafast synthesis of resorcinol-formaldehyde carbon aerogel monoliths. *Carbon* **2022**, *194*, 220–229. [CrossRef]
15. Gan, L.; Zhong, Q.; Geng, A.; Wang, L.; Song, C.; Han, S.; Cui, J.; Xu, L. Cellulose derived carbon nanofiber: A promising biochar support to enhance the catalytic performance of $CoFe_2O_4$ in activating peroxymonosulfate for recycled dimethyl phthalate degradation. *Sci. Total Environ.* **2019**, *694*, 133705. [CrossRef]
16. Geng, A.; Meng, L.; Han, J.; Zhong, Q.; Li, M.; Han, S.; Mei, C.; Xu, L.; Tan, L.; Gan, L. Highly efficient visible-light photocatalyst based on cellulose derived carbon nanofiber/BiOBr composites. *Cellulose* **2018**, *25*, 4133–4144. [CrossRef]
17. Yu, Y.; Liu, Y.; Wu, X.; Weng, Z.; Hou, Y.; Wu, L. Enhanced visible light photocatalytic degradation of metoprolol by Ag–Bi2WO6–graphene composite. *Sep. Purif. Technol.* **2015**, *142*, 1–7. [CrossRef]
18. Jia, H.; Zhao, S.; Zhu, K.; Huang, D.; Wu, L.; Guo, X. Activate persulfate for catalytic degradation of adsorbed anthracene on coking residues: Role of persistent free radicals. *Chem. Eng. J.* **2018**, *351*, 631–640. [CrossRef]
19. Hu, W.; Tong, W.; Li, Y.; Xie, Y.; Chen, Y.; Wen, Z.; Feng, S.; Wang, X.; Li, P.; Wang, Y.; et al. Hydrothermal route-enabled synthesis of sludge-derived carbon with oxygen functional groups for bisphenol A degradation through activation of peroxymonosulfate. *J. Hazard. Mater.* **2019**, *388*, 121801. [CrossRef]
20. Cheng, X.; Guo, H.; Zhang, Y.; Wu, X.; Liu, Y. Non-photochemical production of singlet oxygen via activation of persulfate by carbon nanotubes. *Water Res.* **2017**, *113*, 80–88. [CrossRef]
21. Hou, P.; Xing, G.; Tian, L.; Zhang, G.; Wang, H.; Yu, C.; Li, Y.; Wu, Z. Hollow carbon spheres/graphene hybrid aerogels as high-performance adsorbents for organic pollution. *Sep. Purif. Technol.* **2018**, *213*, 524–532. [CrossRef]
22. Liang, J.; Xu, X.; Zaman, W.Q.; Hu, X.; Zhao, L.; Qiu, H.; Cao, X. Different mechanisms between biochar and activated carbon for the persulfate catalytic degradation of sulfamethoxazole: Roles of radicals in solution or solid phase. *Chem. Eng. J.* **2019**, *375*, 121908. [CrossRef]
23. Pereira, A.T.; Henriques, P.C.; Costa, P.C.; Martins, M.C.L.; Magalhães, F.D.; Gonçalves, I.C. Graphene oxide-reinforced poly(2-hydroxyethyl methacrylate) hydrogels with extreme stiffness and high-strength. *Compos. Sci. Technol.* **2019**, *184*, 107819. [CrossRef]
24. Pan, Y.; Wang, Q.; Zhou, M.; Cai, J.; Tian, Y.; Zhang, Y. Kinetic and mechanism study of UV/pre-magnetized-Fe0/oxalate for removing sulfamethazine. *J. Hazard. Mater.* **2020**, *398*, 122931. [CrossRef] [PubMed]

25. He, J.; Zhou, Q.; Chen, S.; Tian, M.; Zhang, C.; Sun, W. Interfacial microstructures and adsorption mechanisms of benzohydroxamic acid on Pb2+-activated cassiterite (110) surface. *Appl. Surf. Sci.* **2020**, *541*, 148506. [CrossRef]
26. Liu, C.; Liu, L.; Tian, X.; Wang, Y.; Li, R.; Zhang, Y.; Song, Z.; Xu, B.; Chu, W.; Qi, F.; et al. Coupling metal–organic frameworks and g-C3N4 to derive Fe@N-doped graphene-like carbon for peroxymonosulfate activation: Upgrading framework stability and performance. *Appl. Catal. B-Environ.* **2019**, *255*, 117763. [CrossRef]
27. Wang, J.; Wang, S. Preparation, modification and environmental application of biochar: A review. *J. Clean. Prod.* **2019**, *227*, 1002–1022. [CrossRef]
28. Tao, W.; Duan, W.; Liu, C.; Zhu, D.; Si, X.; Zhu, R.; Oleszczuk, P.; Pan, B. Formation of persistent free radicals in biochar derived from rice straw based on a detailed analysis of pyrolysis kinetics. *Sci. Total Environ.* **2020**, *715*, 136575. [CrossRef]
29. Wu, J.; Grant, P.; Li, X.; Noble, A.; Aggarwal, V.K. Catalyst-Free Deaminative Functionalizations of Primary Amines by Photoinduced Single-Electron Transfer. *Angew. Chem. Int. Ed.* **2019**, *58*, 5697–5701. [CrossRef]
30. Duan, X.; Sun, H.; Wang, S. Metal-Free Carbocatalysis in Advanced Oxidation Reactions. *Acc. Chem. Res.* **2018**, *51*, 678–687. [CrossRef]
31. Liu, J.; Huang, S.; Chen, K.; Wang, T.; Mei, M.; Li, J. Preparation of biochar from food waste digestate: Pyrolysis behavior and product properties. *Bioresour. Technol.* **2020**, *302*, 122841. [CrossRef]
32. Han, R.; Fang, Y.; Sun, P.; Xie, K.; Zhai, Z.; Liu, H.; Liu, H. N-Doped Biochar as a New Metal-Free Activator of Peroxymonosulfate for Singlet Oxygen-Dominated Catalytic Degradation of Acid Orange 7. *Nanomaterials* **2021**, *11*, 2288. [CrossRef]
33. Hu, Y.; Chen, D.; Zhang, R.; Ding, Y.; Ren, Z.; Fu, M.; Cao, X.; Zeng, G. Singlet oxygen-dominated activation of peroxymonosulfate by passion fruit shell derived biochar for catalytic degradation of tetracycline through a non-radical oxidation pathway. *J. Hazard. Mater.* **2021**, *419*, 126495. [CrossRef]
34. Lata, H.; Garg, V.; Gupta, R. Adsorptive removal of basic dye by chemically activated Parthenium biomass: Equilibrium and kinetic modeling. *Desalination* **2008**, *219*, 250–261. [CrossRef]